IEEE Access
Multidisciplinary | Rapid Review | Open Access Journal

Received September 22, 2021, accepted October 24, 2021, date of publication October 27, 2021, date of current version November 9, 2021.

Digital Object Identifier 10.1109/ACCESS.2021.3123471

Frequency Adaptive Topology to Realize Constant Output and Soft Switching for the WPT System

BING CHENG AND LIANGZONG HE
Electrical Engineering Department, University of Xiamen, Xiamen 361012, China
Corresponding author: Liangzong He (hlz190213@163.com)

This work was supported in part by the National Natural Science Foundation Project under Grant 62071406, and in part by the Natural Science Foundation of Guangdong Province General Project under Grant 2021A1515011710.

ABSTRACT The main emphasis of research for battery wireless charger should be on four parts, including load-independent output to satisfy the charging requirement, zero voltage switching of power devices to increase transmission efficiency, minimum component counts to reduce cost and simple control strategy. However, the existing studies have not taken these all into account, which greatly limits the application of battery wireless charger. This paper proposes a WPT system based on the simplest S/S compensation network. By replacing the secondary compensation capacitor with an *L*-*C* branch, the same circuit structure can realize the load-independent constant current (CC) and voltage (CV) output with zero voltage switching at two different switching frequency. A current amplitude detection circuit is added in the primary side to determine the switching point of CC mode and CV mode. Compared with existing research, the component numbers in proposed circuit are less, the control strategy is easier to implement and avoids the communication between the primary and secondary sides. Finally, a wireless battery charger for 60V/3.6A is built to verify the feasibility of proposed system. And the experimental results perform well on realizing a load-independent output with ZVS operation.

INDEX TERMS Wireless power transfer (WPT), adaptive branch, load estimation, load-independent output, zero voltage switching (ZVS).

I. INTRODUCTION

Nowadays, the traditional connecting way by wires makes the life more and more tedious with the developing of electrical devices. By comparison, wireless power transfer (WPT) technology has attracted more and more attention due to its flexibility, convenience and safety. And it has huge application value and potential in various fields, such as biomedical implants [1], [2], daily electrical consumption [3] and electrical vehicle [4]–[6]. Among them, the battery serves as a very important part of energy storage system, a lot of researches on the battery wireless charger have been done. The typical charging curve for lithium battery is shown in Fig.1 [7]. From Fig. 1, the wireless power charger should work at constant current (CC) mode first and then the constant voltage (CV) mode. The large charging current at the CC mode can reduce the charging time. The constant charging voltage at the CV mode will ensure the battery is full charged. Besides, the equivalent battery impedance (EBI) is increasing with the charging process going on. Therefore, according to the charging curve, load-independent current and voltage output are the focus of research.

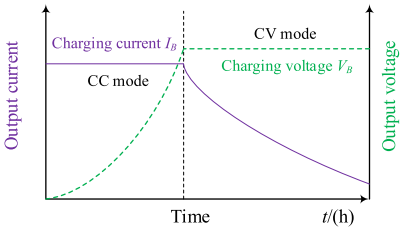

FIGURE 1. The typical charging curve for lithium battery.

Various control strategies have been investigated to realize CC or CV output in the past few years [8], [9]. The operating frequency adjustment strategy is adopted to realize a CC and CV output for the LLC resonant converter [10], however, if the load varies seriously, the frequency needs to be adjusted over a wide range and the system stability will be killed due to the frequency bifurcation phenomenon. Two dc/dc converters are normally controlled cooperatively for the requirements of output regulation and maximum efficiency tracking [11], however, system size and cost will increase due to the existing

The associate editor coordinating the review of this manuscript and approving it for publication was Chi-Seng Lam.

of additional converter. Meanwhile, the system transmission efficiency will be affected by the power loss of extra components. In [12], the phase shift angle tracking strategy can compensate the effect of variations to output current until the output current equals the desired output, however, the control strategy requires a communication between the primary side and secondary side. Besides, the ZVS condition is hard to maintain if the phase shift angle is too large. The load-independent constant output can be realized without additional components component counts according to the proper design of the compensation network [13], however, the existing compensation network needs too many passive components, which to some degree reduces its practicality.

When it comes to the switching method from CC mode to CV mode, changing the circuit compensation network structure by adding additional AC switches is proposed in [14] and [15], The charging current and charging voltage are nearly constant during the transient switching interval. However, the additional AC switches will increase the system cost and the corresponding driving circuits will also make the whole circuit bulky. An integrated IPT system design employing variable inductor control is proposed to achieve a target constant current (CC) and constant voltage (CV) battery charging profile with misalignment tolerance [16], however, the realization of variable inductor needs an addition of BUCK converter, which increases the complexity of control process. By comparison, the realization of the CC and CV charging modes at two fixed operation frequencies is more acceptable.

Based on the above analysis, this paper presents a two-coil structure WPT system based on the improved S/S compensation network. The improvement of S/S compensation network makes it possible to realize the CV and CC charging modes with the ZVS condition at two different operation frequencies, respectively. The switching point of two charging mode can be obtained according to a current detection circuit, which avoids the communication between the primary and secondary sides. And the adjustment of operation frequency can be executed in the DSP, which avoids the addition of redundant segments.

The paper is organized as follows. Section II analyzes the load-independent output characteristics of the simple compensation network, and then proposes a simplest and desired compensation network structure. In Section III, the parameters design, verification of load-independent output characteristics, test of robustness performance and comparison with other counterparts are given. Then follows the experimental part in Section IV. Finally, the Section V is the conclusion content.

II. LOAD-INDEPENDENT CC AND CV OUTPUTS WITH ZVS OPERATION

A. DERIVATION OF SIMPLEST COMPENSATION NETWORK TO REALIZE LOAD-INDEPENDENT CC OUTPUT

As shown in Fig. 2, the S/S compensation network is widely used in wireless power transfer system. The V_s and i_T represent the input AC voltage and current, respectively. Similarly, the V_o and i_R are the output AC voltage and current, respectively. The L_p is the self-inductance of transferring coil and L_s is that of receiving coil. M is determined by the transmission distance of coupling coils and reflect the coupling ability. R_L is an ac load. The R_p is the series internal resistor of L_p-C_p branch and R_s is the series internal resistor of L_s-C_s branch. The C_p and C_s are the corresponding compensation capacitors in the primary and secondary side, respectively. And the value of them are chosen to meeting the circuit requirements.

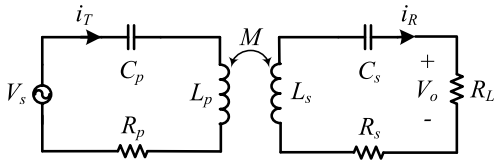

FIGURE 2. The simplest compensation network used in wireless power transfer system.

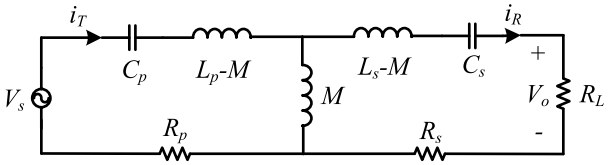

FIGURE 3. The equivalent circuit based on the mutual inductance theory.

According to the mutual inductance theory, the circuit in Fig. 2 can be equivalent to the circuit in Fig. 3. And then based on the Kirchhoff voltage Law (KVL), the mathematical expression of the circuit can be given as

$$\begin{cases} V_s = (1/(j\omega_1 C_p) + j\omega_1 L_p + R_p) i_T - j\omega_1 M i_R \\ 0 = (1/(j\omega_1 C_s) + j\omega_1 L_s + R_s + R_L) i_R - j\omega_1 M i_T \end{cases} \tag{1}$$

where the ω_1 means the resonant angle frequency in load-independent CC mode.

When the following conditions are given

$$Z_T = 1/(j\omega_1 C_p) + j\omega_1 L_p = 0 \tag{2}$$

$$Z_R = 1/(j\omega_1 C_s) + j\omega_1 L_s < 0 \tag{3}$$

The relationship between the output current and input voltage is derived as

$$V_{in} = \frac{(Z_R + R_s + R_L)R_p + \omega_1^2 M^2)}{j\omega_1 M} i_R \tag{4}$$

From (4), i_R is related to the load R_L due to the existence of R_p. However, the R_p is quite small, the difference caused by the R_p and R_s can be ignorable during the CC charging mode. Finally, the output current can be simplified as

$$i_R = V_s/(\omega_1 M) \tag{5}$$

In addition, the input impedance of given circuit is expressed without the consideration of R_p and R_s

$$Z_{inc} = Z_T + \omega_1^2 M^2/(Z_R + R_L) \tag{6}$$

Moreover, under the conditions (2) and (3), Z_{inc} is given by

$$Z_{inc} = \frac{\omega_1^2 M^2 (R_L - Z_R)}{(|Z_R|)^2 + R_L^2} \tag{7}$$

Therefore, the input impedance Z_{inc} is inductive no matter how R_L changes. Further, the power devices of high frequency inverter can realize the ZVS turn-on to improve transmission efficiency in the whole CC mode.

B. DERIVATION OF SIMPLEST COMPENSATION NETWORK TO REALIZE LOAD-INDEPENDENT CV OUTPUT

The similar analysis process can be used in the load-independent CV output mode. The KVL equation can be changed into (8), which is shown as follows

$$\begin{cases} V_s = (1/(j\omega_2 C_p) + j\omega_2 L_p + R_p) i_T - j\omega_2 M i_R \\ V_o = (1/(j\omega_2 C_s) + j\omega_2 L_s + R_s) i_R - j\omega_2 M i_T \end{cases} \tag{8}$$

where the ω_2 is the resonant angle frequency in load-independent CV mode.

Then the relationship between the output AC voltage and input AC voltage is given as

$$\frac{V_s}{V_o} = \frac{(1/(j\omega_2 C_p) + j\omega_2 L_p + R_p) i_T - j\omega_2 M i_R}{(1/(j\omega_2 C_s) + j\omega_2 L_s + R_s) i_R - j\omega_2 M i_T} \tag{9}$$

In (9), if the R_p and R_s are overlooked, with the following condition

$$(\omega_2 L_p - 1/(j\omega_2 C_p))(\omega_2 L_s - 1/(j\omega_2 C_s)) = \omega_2^2 M^2 \tag{10}$$

The output voltage is load-independent, and the expression of output voltage yields as

$$\frac{V_s}{V_o} = \frac{\omega_2 L_p - 1/(\omega_2 C_p)}{\omega_2 M} \tag{11}$$

Furthermore, according to (10), the input impedance of given circuit Z_{inv} is expressed as

$$Z_{inv} = \frac{\omega_2^2 M^2 R_L + j R_L^2 (\omega_2 L_p - 1/(\omega_2 C_p))}{(\omega_2 L_s - 1/(\omega_2 C_s))^2 + R_L^2} \tag{12}$$

Obviously, with the follow condition

$$\omega_2 L_p - 1/(\omega_2 C_p) > 0 \tag{13}$$

The input impedance Z_{inv} is inductive and the ZVS turn-on is realized during the CV mode too. Besides, to satisfy the (10) and (13) simultaneously, the C_s in the secondary side should be an inductor L_1, and its value is independent on the ω_2.

C. DERIVATION OF SIMPLEST COMPENSATION NETWORK TO REALIZE LOAD-INDEPENDENT CV/CC OUTPUT

Based on the analysis result in Section A and B. The same compensation network structure can realize the load-independent output voltage and current at two different operation angle frequency ω_1 and ω_2. However, the load-independent ZVS condition cannot be achieved in CC and CV modes simultaneously. To solve this problem, an adaptive branch L_r-C_r is used to replace the capacitor C_s. And the equivalent impedance of this branch will change with the variation of operation frequency. The function of adaptive branch is equivalent as a capacitor C_s in operation frequency f_1 and an inductor L_1 in operation frequency f_2. The equivalent impedance of this branch against the operation frequency is drawn as shown in Fig. 4. The branch inductance L_r and capacitor C_r will be determined once the capacitor C_s in operation frequency f_1 and the inductor L_1 in operation frequency f_2 are given. The relationship among them can be expressed as

$$\begin{cases} -1/(\omega_1 C_s) = \omega_1 L_r - 1/(\omega_1 C_r) \\ \omega_2 L_1 = \omega_2 L_r - 1/(\omega_1 C_r) \end{cases} \tag{14}$$

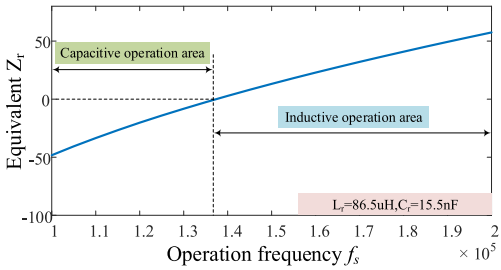

FIGURE 4. The equivalent impedance of this branch against the operation frequency f_s.

Then the value of inductance L_r and capacitor C_r are obtained as

$$\begin{cases} C_r = \dfrac{C_s(\omega_2^2 - \omega_1^2)}{\omega_2^2(1 + \omega_1^2 L_1 C_s)} \\ L_r = \dfrac{\omega_2^2 L_1 C_s + 1}{C_s(\omega_2^2 - \omega_1^2)} \end{cases} \tag{15}$$

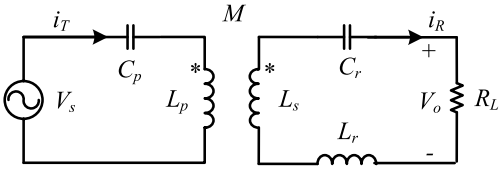

FIGURE 5. The chosen compensation network to realize the load-independent CC/CV output with ZVS condition.

The compensation network to realize the load-independent CC output with ZVS condition and CV output with ZVS condition at two different operation frequencies is drawn in Fig. 5. When the operation frequency is f_1, the whole circuit works at CC mode and the L_r-C_r branch is equivalent to a capacitor, the ZVS of power devices of high frequency inverter is realized. To obtain a CV output with ZVS condition, the operation frequency is changed to f_2. At present, the L_r-C_r branch can be seen as an inductor. In short, the ZVS condition can be satisfied during the whole charging process.

III. EVALUATIONS

Based on the analysis result in Section II, the topology to realize the load-independent current and voltage output with ZVS condition under two different operation frequencies is given in Fig. 6.

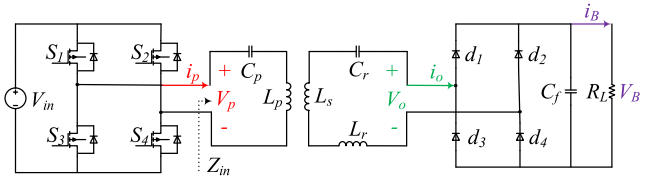

FIGURE 6. Schematic for the proposed WPT system with adaptive branch.

A. PARAMETER DESIGN

The output and input characteristics are determined by the circuit parameters. Therefore, a detailed flowchart to describe the design procedure of the system parameters is presented in Fig.7. And the detailed introduction is given below.

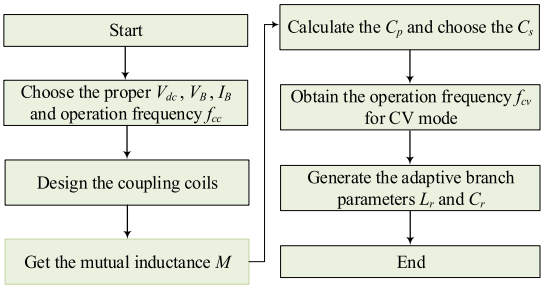

FIGURE 7. The parameters design procedure of the proposed system.

Firstly, the load-independent CC operation frequency f_{cc} is set. Then based on the battery datasheet, the charging voltage and current are given. And the relationship between the input and the output of rectifier can be derived with the following equations [17]

$$V_o = \frac{2\sqrt{2}V_B}{\pi}$$
$$I_o = \frac{\pi\sqrt{2}I_B}{4} \tag{16}$$

The output voltage V_p of the H-bridge inverter can be controlled by adopting the phase shift angle adjustment and the dc voltage V_{dc}. The fundamental component magnitude V_p of inverter output voltage with zero phase shift can be expressed as

$$V_p = \frac{2\sqrt{2}V_{dc}}{\pi} \tag{17}$$

Reasonable coil design will promote the improvement of system transmission efficiency and output power, simultaneously, the size, weight and cost of the coils will be reduced as well [18]. The spiral coil structure is chosen due to the stronger coupling coefficient under the same working condition. The Litz wire is used to weaken the skin effect and further abate the ac resistance value. The transmitting coil and receiving coil adopt the same structure and design parameters, which can reduce the production cost and ensure the consistency of parameters for resonance. The coil model is analyzed by Ansoft Maxwell to estimate its self-inductance. Simultaneously, Fig 8 shows the curve of coupling coefficient k with the transmission distance d. the experimental value of M is obtained by open circuit voltage. And the curve in Fig. 8 would be a reference to determine the transmission distance for required output.

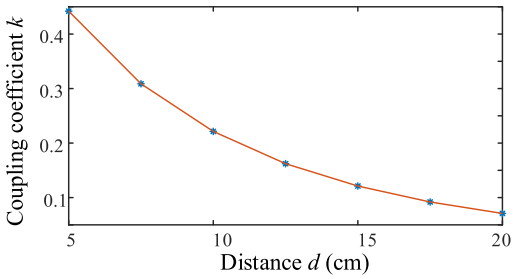

FIGURE 8. The coupling coefficient k against the coils distance d.

Based on the analysis in Section II, from (2), the compensation capacitor C_p in the primary side can be derived. The value of C_s has an important influence on the circuit performance of proposed system, therefore, the C_s should be set as large as possible under the condition (3).

The transmission of working mode is implemented by changing the working frequency of HFI. The resonant frequency f_{cc} at the CC mode has been already set. The relationship between the circuit parameters and operation frequency f_{cv} at CV mode is obtained in equation (10), then the operation frequency f_{cv} can be deduced as

$$f_{cv} = \frac{1}{2\pi}\sqrt{\frac{M + L_{eq}}{(ML_{eq}C_p + C_p(L_p - M)(L_{eq} + M)}} \tag{18}$$

where the L_{eq} is represented as

$$L_{eq} = \frac{M(V_o - V_p)}{V_p} \tag{19}$$

The adaptive branch parameters are related with the two operation frequency f_{cc} and f_{cv}. And the expression is already given in equation (15). The circuit parameters of the designed WPT system obtained based on the aforementioned design flow are provided in Table 1. During the parameter design process, the mutual inductance M is fixed. The variation of M due to the coils misalignment will affect the load-independent voltage output characteristic. It will be given full consideration in future work.

B. THE VERIFICATION OF LOAD-INDEPENDENT OUTPUT AND INPUT IMPEDANCE CHARACTERISTICS

It is crucial to verify the rationality of the parameters design method for the proposed two-coil WPT system.

TABLE 1. Parameters for the proposed hybrid WPT system.

Parameter	Designed value	Measured value
Operation frequency f_{cc}	100kHz	100kHz
Operation frequency f_{cv}	115.55khz	115khz
Self-inductance L_p	57.8uH	57.8uH
Self-inductance L_s	58.04uH	58.04uH
Resonant capacitor C_p	43.999nF	43.775nF
Adaptive capacitor C_r	15.508nF	14.952nF
Adaptive inductor L_r	86.578uF	86.45uH
Distance d	7cm	7cm
Self-resistances R_p/R_s	0.124/0.129Ω	0.124/0.129Ω
Coupling coefficient k	0.3101	0.3101
Output parameter V_B/I_B	60V/3.6A	60V/3.6A

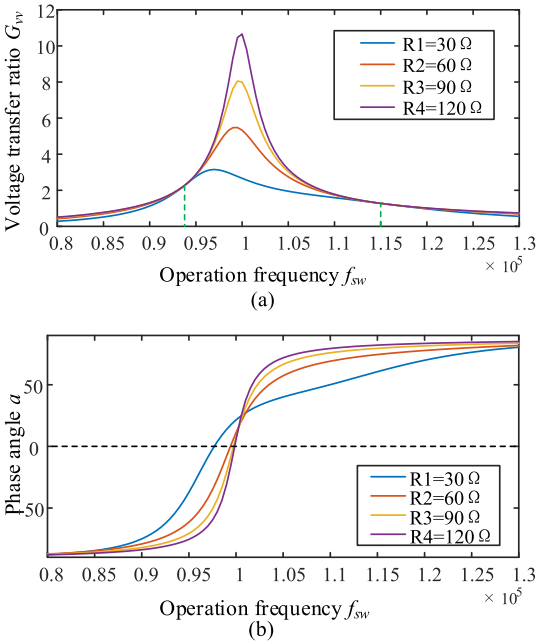

FIGURE 9. The curves of the voltage transfer ratio and the phase angle of the related input impedance Z_{inv} versus frequency at different load conditions.

The parameters in Table 1 are adopted to verify the output and input characteristics. The curves of the voltage transfer ratio G_{vv} and the phase angle a of the Z_{inv} versus frequency at different load conditions are shown in Fig. 9. As shown in Fig. 9(a), there are two switching frequency points (93 kHz and 115 kHz), where the output voltage is both load-independent. However, according to Fig. 9(b), the phase angle at the first frequency point (93 kHz) is negative, which means the ZVS condition of the HFI is not satisfied. Therefore, the frequency 93 kHz will be abandoned. On the contrary, the ZVS is achieved at the frequency point (115 kHz) due to the positive phase angle value. Therefore, the frequency point (115 kHz) is selected as the operation frequency at CV mode. And the G_{vv} in the frequency point (115 kHz) is 1.199, which agrees well with the theoretical analysis result. The graphs of the current transfer ratio G_{cv} and the phase angle of the corresponding input impedance Z_{inc} under different loads are illustrated in Fig. 10. It can be seen that the load-independent current output and ZVS condition are both satisfied at the set resonant frequency 100 kHz. And the current transfer ration G_{cv} in 100 kHz is 0.0883, which is the ratio of output current to input voltage. As a conclusion of the figures in Fig. 9 and Fig. 10, the design procedure in Fig. 7 can enable the proposed topology to obtain the desired load-independent CC and CV output characteristics as well as the associated ZVS conditions at two fixed switching frequency points, respectively.

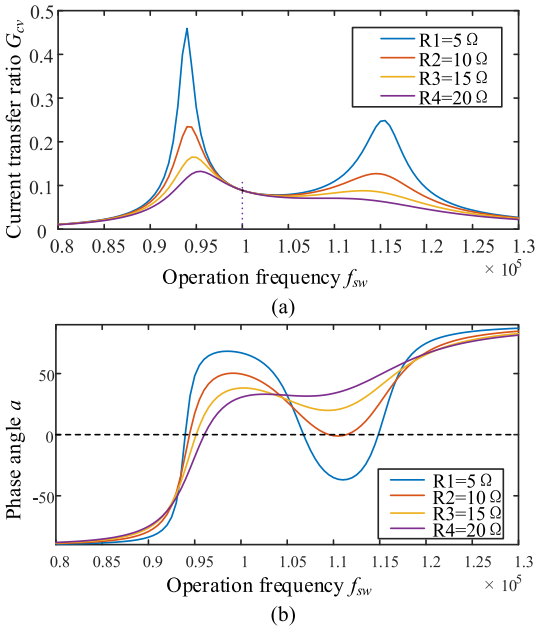

FIGURE 10. The curves of the current transfer ratio and the phase angle of the related input impedance Z_{inc} versus frequency at different load conditions.

TABLE 2. The ESR of used passive components.

Parameter	Designed value	Measured value
C_p	43.999nF	0.02Ω
L_p	57.57uH	0.124Ω
L_s	57.98uH	0.129Ω
C_r	15.508nF	0.019Ω
L_r	86.578uH	0.156Ω

C. THE ROBUSTNESS ANALYSIS COMES FROM THE ESRS OF THE CAPACITORS AND INDUCTANCES

In the practical application, the equivalent series resistances (ESRs) of the inductors and capacitors are inevitable. The influence comes from them should be taken into consideration. The ESR values of adopted passive components are given in Table 2. The output and input characteristics without ESRs are analyzed by simulation due to the absence of ideal passive components in practical. The normalized output voltage and input impedance angle curves in CV mode are drawn in Fig. 11(a) and Fig. 11(b), respectively. According to the comparison result in Fig. 11(a), the output voltage will be affected by the ESRs. Normally, the output voltage will

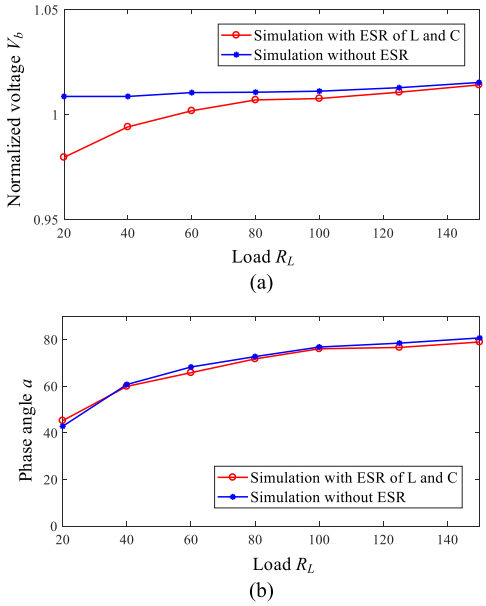

FIGURE 11. The normalized output voltage and input impedance angle curves in CV mode.

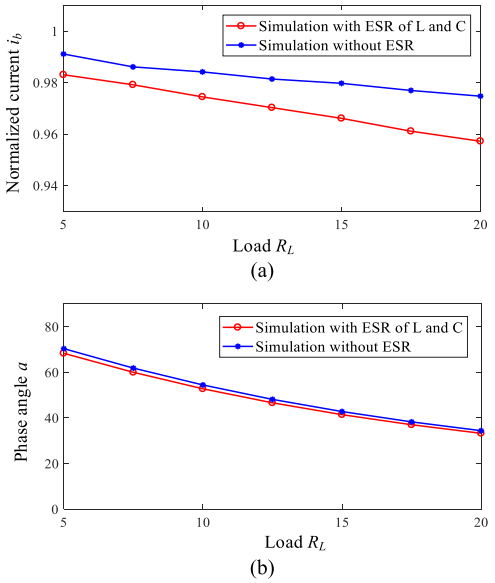

FIGURE 12. The normalized output voltage and input impedance angle curves in CV mode.

decrease due to the existing of ESRs. And the maximum difference happens when the load value is minimum. The reason is that the ESRs will lead a voltage drop during the whole transmission process. However, the difference is so small that it is acceptable in practical occasion. Similarly, the input impedance angle will be affected by the ESRs. Yet the input impedance angle is still positive, therefore, the ZVS of HFI will maintain in practical application. The Fig. 12 shows the normalized current output and input impedance angle curve against the load when the ESRs is considered or not. From Fig. 12(a), when the ESRs are added in the simulation system, the output current will decrease. Moreover, the difference value will increase with the increasing of load and the maximum error ratio is 1.75% at the crossing point of two charging mode. Similar with the input characteristic at CV mode, the ESRs will affect the input impedance angle but not change the positive or negative characteristics. In other words, the ZVS condition will not be affected by the ESRs. In short, the ESRs of passive components will cause some influence to the output and input characteristics but they are acceptable in practical.

D. THE COMPARISON WITH THE OTHER COUNTERPARTS

A lot of papers have been done on the research of the battery wireless charger. Normally, when the system is adopted, the system size and cost are focus of concern. The composition of the compensation network part in serval counterparts [14], [17]–[20] are making a comparison in Table 3. The application of multi-coil to realize a CC or CV output can increase the coupling ability, however, it takes up a lot of space and increases the system cost. Among the two-coil system, the proposed converter only uses one inductor, hence, the power density of whole system can be very high.

TABLE 3. Comparison with different papers for load-independent CC and CV outputs with ZVS condition.

	Coils	Capacitors	inductors	Additional switches	ZVS
[14]	4	4	0	2	√
[19]	2	4	1	2	√
[20]	3	5	1	2	ZPA
[21]	2	4	2	0	√
[22]	3	3	0	0	√
Proposed	2	2	1	0	√

Simultaneously, it also has the least amount of capacitor. As a result, the cost in proposed converter can be cut down greatly. In addition, there is no additional switches used in proposed topology. In [20], the switch connected with a passive component may have potential danger when the switch turns off with residual energy. The parasitic parameters of the switches will also have an important influence on the system performance. In sum, the proposed converter performs better in the comprehensive performance of the system when the load-independent CC and CV output with ZVS condition is required for wireless battery charger.

E. CONTROL STRATEGY

Based on the parameters design procedure, the proposed topology can realize load-independent CC output and CV output with ZVS condition at two different operation frequencies, respectively. During the battery charging process, the whole system works at CC mode firstly and then the CV mode. The transparent signal of the switching point from CC mode to CV mode is that the output voltage reaches the preset charging voltage in CV mode, or the equivalent battery internal resistance rises to R_{set}, the equivalent battery internal

resistance can be evaluated by detecting the input current i_p.

$$R_{set} = \frac{V_B}{i_B} \tag{20}$$

$$Z_{inc} = \frac{\omega_1^2 M^2}{R_{set} + j(\omega_1 L_s - 1/(\omega_1 C_r) + \omega_1 L_r)} \tag{21}$$

$$|I_{set}| = \frac{V}{|Z_{inc}|} \tag{22}$$

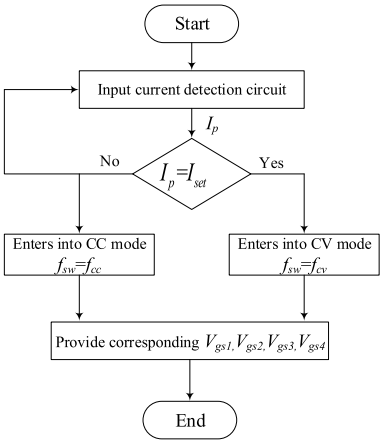

FIGURE 13. Control diagram for the proposed topology.

The control diagram for the proposed WPT system is provided in Fig. 13, where I_p and I_{set} are the input current magnitude and reference current corresponding to the R_{set}, respectively. A current detective circuit is introduced to measure the magnitude of input current i_p. The resonant tank current in the primary side is converted into ac voltage signal by a Hall current sensor HBC-ES3.3, then an RMS calculator AD637 is employed to obtain the effective value V_odc of ac voltage signal. Then the V_odc is sent into the digital-signal processor TMS320F28335. When the input current magnitude I_p is smaller than the reference charging current I_{set}, the operation frequency is chosen as f_{cc} to work at CC mode. When input current magnitude I_p reaches the reference charging current I_{set} during the charging process, the operation frequency is adjusted to f_{cv}. The charging mode will be changed to CV mode by changing the operation frequency to f_{cv}.

The proposed WPT system can operate in CC mode or CV mode by changing the operation frequency of HFI, and both two operation modes can achieve ZVS. The performance comparison on the control strategy is presented in Table 4. Compared with [17], [20] and [21], there is no communication between the primary side and secondary side in the proposed WPT system, which can not only save the cost but also avoid the error caused by the instability of wireless communication. Meanwhile, the input current magnitude I_p is the only variable required to be measured. The detection execution in the proposed system will become simpler than the detection circuits in [22]–[26]. In general, the control strategy is easy, simple and economical to implement in practical application for battery charger.

TABLE 4. Comparison with different papers in control strategy.

	Measured parameters	communication	Implementation
[23]	i_{Bat}, V_{Bat}	×	middle
[24]	U_c, I_c	√	complex
[25]	U_{inv}, i_{inv}	×	complex
[14]	V_B	√	middle
[22]	U_B, I_B	√	complex
[26]	U_i, I_i	×	complex
Proposed	i_p	×	easy

The * means the parameters are not given in the paper.
The √ means the communication between the transmitter side and the receiving side is needed.
The × means the communication between the transmitter side and the receiving side is not needed.

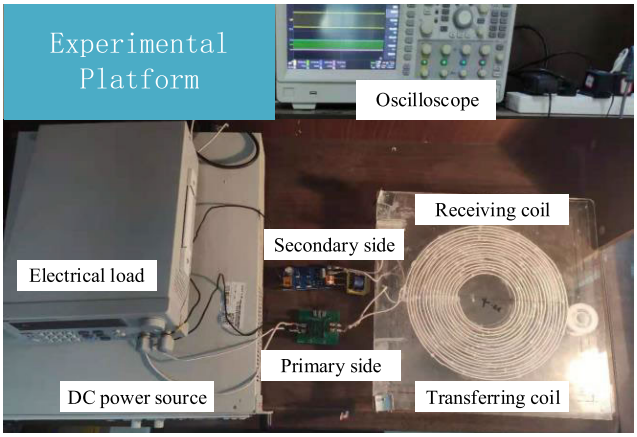

FIGURE 14. Experimental platform of the proposed two-coil WPT system.

IV. EXPERIMENTAL RESULTS

To verify the feasibility of the theoretical analysis, an experimental platform with 60V charging voltage and 3.6A charging current output based on the proposed circuit structure is built in Fig. 14. The component parameters in Table 1 are used. It is need to say that the experimental setup is constructed to confirm the practicability of proposed circuit topology and control strategy. The whole experimental prototype can be adjusted properly when it is adopted to different applications.

A. EXPERIMENTAL PLATFORM

In the experimental platform, in the primary HFI part, the Infineon IRFP4227 is adopted due to its low conduction resistance in high frequency occasions. the gate driving chip SI8233BD is chosen to drive the MOSFETs. The full bridge rectifier in the secondary side is constructed by the Schottky diode PSM20U200GS. The polypropylene film capacitor is adopted as the compensation capacitor due to its stability in high frequency condition. Simultaneously, multiple nominal capacitors are connected in parallel, as a result, the equivalent

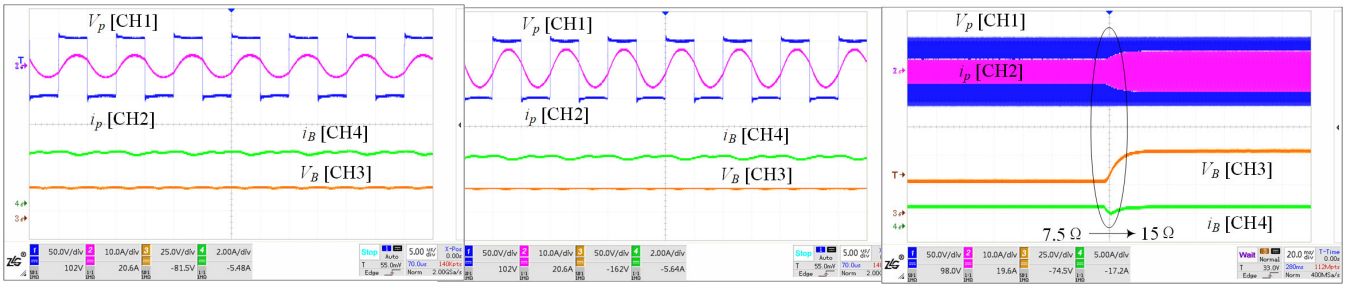

FIGURE 15. The waveforms at the CC mode. (a) When $R_L = 7.5\Omega$. (b) When $R_L = 15\Omega$. (c) Transient waveforms of load changes from 7.5Ω to 15Ω.

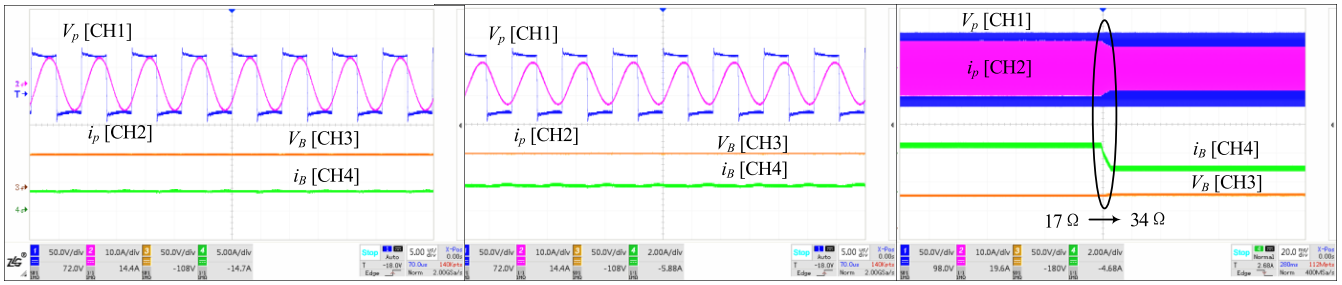

FIGURE 16. The waveforms at the CV mode. (a) When $R_L = 17\Omega$. (b) When $R_L = 34\Omega$. (c) Transient waveforms of load changes from 17Ω to 34Ω.

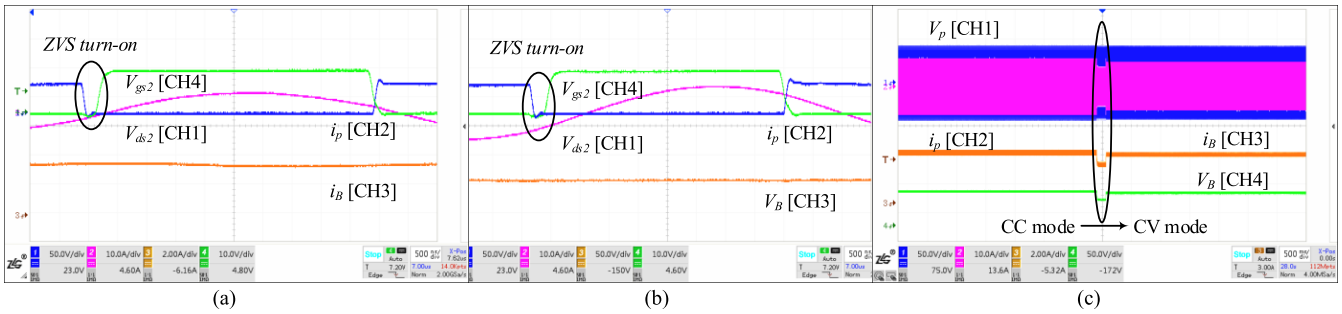

FIGURE 17. The waveforms at switching point. (a) ZVS at CC mode. (b) ZVS at CV mode. (c) Transient waveforms of mode switching from CC to CV mode.

series resistance in practical application is reduced, and the capacitor value error between the designed and measured resonant capacitor value can be diminished to near zero. As for the resonant inductor L_r, the magnetic core material is preferably ferrite material with lower loss and the Litz wire is extremely suited due to its lower skin effect loss and smaller equivalent series resistance in high frequency occasion. The electronic load is used to imitate the changing equivalent battery internal resistor during the charging process.

B. EXPERIMENTAL RESULTS

When the charging process starts, the system works at the CC mode firstly. The waveforms of input current i_p, input voltage V_p, output current i_B and output voltage V_B in 7.5Ω and 15Ω are shown in Fig. 15(a) and Fig. 15(b), respectively. As shown in Fig 15(a) and Fig. 15(b), the resonant frequency is 100 kHz and the output current maintains 3.6A. Besides, the waveforms of S_2 are shown in Fig. 17(a), the input current lags input voltage by tens of degrees, therefore, the reverse parallel body diode of S_2 is turned on, and the voltage V_{ds2} is choked as the forward conduction voltage drop of the parallel body diode. Hence, the crossing area of V_{ds2} and i_p is close to zero, which means the ZVS for S_2 has been realized. The other switches have the same working principle with S_2. The transient waveforms of load changing from 7.5Ω to 15Ω at the CC mode are shown in Fig. 15(c). It is obvious that the charging current remains almost constant after a small overshoot. The slight output current error happens due to the unideal devices in practical experimental setup. And the difference is so small that it can be negligible.

The output voltage changes proportionally with the load at the CC mode. The whole system enters into CV mode when the output voltage reaches 60V. The switching point is determined by the measurement of input current amplitude. The transient waveforms of mode switching from CC mode to CV mode are given in Fig. 17(c). From Fig. 17(c), the response is fast and the charging voltage and current will return to normal after a small drop happens. In addition,

since there is difference between the equivalent circuits in CC and CV mode, the amplitude of input current in two modes are different. Moreover, there is no voltage and current spike during the switching process, compared with the other switching way by controlling additional switches, Good stability and safety makes it more practical in battery charging application.

The whole system works at CV mode until the end of charging process. The waveforms of input current i_p, input voltage V_p, output current i_B and output voltage V_B in 17Ω and 34Ω are shown in Fig. 16(a) and Fig. 16(b), respectively. The resonant frequency is around 115 kHz and the output voltage is hold at ∼ 60V. Once again, the waveforms of S_2 at CV mode are shown in Fig. 17(b), the V_{ds2} has been dropped to zero before the V_{gs2} is given, the ZVS is realized for all switches due to the inductive input impedance. Besides, the V_{ds} raise from zero when S_2 is turned off due to the existing of C_{oss}. As a result, the quasi ZVS turn-off is also thought to be realized. Similarly, to test the response performance of the proposed system at the moment of load changes, the corresponding waveforms of load changing from 17Ω to 34Ω are shown in Fig. 16(c). Obviously, the output voltage has almost no change and the output current slowly drops by half. There is no voltage or current spike during the switching process, meaning a good stability.

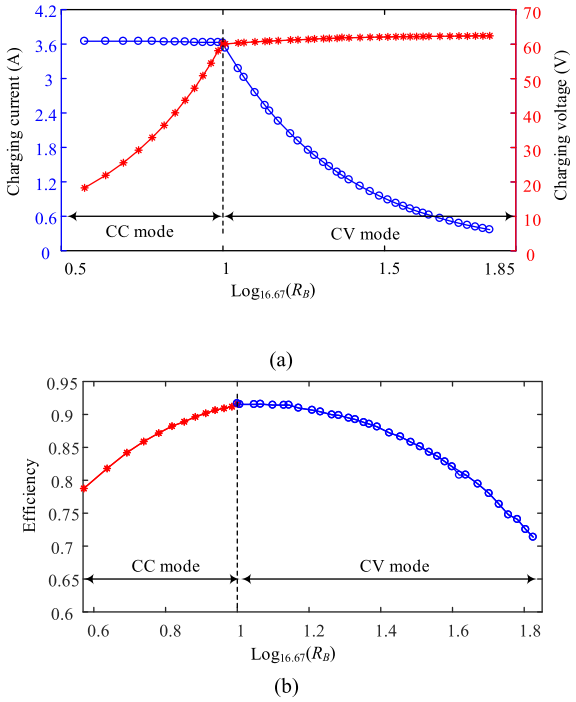

FIGURE 18. Experimental result. (a) Output curve. (b) Efficiency curve.

The measured output voltage and current curves are put in Fig. 18(a). From the Fig. 18(a), the output current has a slight downward trend with the increasing of battery internal resistor in CC mode. When the circuit enters into CV mode, the output voltage increases slowly with the charging process going on. Nevertheless, the highest output voltage at the end point of charging process is 62.4V, which is 4% of rated output voltage. According to the parameter ''Float charging Voltage'' in the datasheet of Lead-Acid battery, the variation voltage value is proper. The transmission efficiency (from the DC source to the battery load) curve versus Log(R_B) is drawn in Fig. 18(b). The transmission efficiency rises up at the CC mode with the increasing of output power, and then it decreases at the CV mode with the decreasing of charging power. The peak efficiency in CC mode and CV mode are up to 91.6% and 91.66%, respectively. Besides, the peak efficiency happens in the crossing point of CC mode and CV mode. Additionally, the charging process comes to an end when the output current reaches one in ten constant charging current in CC mode and the lowest efficiency is 71.37% at this time, which is mainly because that the WPT system works in light-load conditions.

V. CONCLUSION

To increase the system power density and reduce the system cost, the detailed analysis of the simplest S/S compensation network on load-independent output with ZVS is given. Then the WPT system with an adaptive L_r-C_r branch is proposed. The CC mode and CV mode are realized at two different resonant frequencies, respectively. In addition, the influence comes from the ESR of passive component are taken full consideration, which proves the strong robustness of proposed wireless charger. an input current detection circuit is added in the primary side to seek the switching point of two working mode, which avoids the communication between the transfer side and receiver side. Moreover, the good sinusoidal performance of input current waveform makes the error of estimation very small. Finally, the peak transmission efficiency reaches 91.66% and the average transmission efficiency is at a high level due to the ZVS realization during the full charging process. The experimental results are consistent with the theoretical analysis and verify the expected circuit performance. In sum, the proposed WPT system has the advantages of high power density, low system cost and higher transmission efficiency.

REFERENCES

[1] H. Liu, Q. Shao, and X. Fang, ''Modeling and optimization of class-E amplifier at subnominal condition in a wireless power transfer system for biomedical implants,'' *IEEE Trans. Biomed. Circuits Syst.*, vol. 11, no. 1, pp. 35–43, Feb. 2017.

[2] C. Kim, J. Park, S. Ha, A. Akinin, R. Kubendran, P. P. Mercier, and G. Cauwenberghs, ''A 3 mm × 3 mm fully integrated wireless power receiver and neural interface system-on-chip,'' *IEEE Trans. Biomed. Circuits Syst.*, vol. 13, no. 6, pp. 1736–1746, Dec. 2019.

[3] J. Kim, H.-C. Son, D.-H. Kim, and Y.-J. Park, ''Optimal design of a wireless power transfer system with multiple self-resonators for an LED TV,'' *IEEE Trans. Consum. Electron.*, vol. 58, no. 3, pp. 775–780, Aug. 2012.

[4] S. Li and C. C. Mi, ''Wireless power transfer for electric vehicle applications,'' *IEEE J. Emerg. Sel. Topics Power Electron.*, vol. 3, no. 1, pp. 4–17, Mar. 2015.

[5] Z. Yan, B. Song, Y. Zhang, K. Zhang, Z. Mao, and Y. Hu, ''A rotation-free wireless power transfer system with stable output power and efficiency for autonomous underwater vehicles,'' *IEEE Trans. Power Electron.*, vol. 34, no. 5, pp. 4005–4008, May 2019.

[6] J. Pries, V. P. N. Galigekere, O. C. Onar, and G.-J. Su, "A 50-kW three-phase wireless power transfer system using bipolar windings and series resonant networks for rotating magnetic fields," *IEEE Trans. Power Electron.*, vol. 35, no. 5, pp. 4500–4517, May 2020.

[7] A. Khaligh and Z. Li, "Battery, ultracapacitor, fuel cell, and hybrid energy storage systems for electric, hybrid electric, fuel cell, and plug-in hybrid electric vehicles: State of the art," *IEEE Trans. Veh. Technol.*, vol. 59, no. 6, pp. 2806–2814, Jul. 2010.

[8] X. Xie, C. Xie, and L. Li, "Wireless power transfer to multiple loads over a long distance with load-independent constant-current or constant-voltage output," *IEEE Trans. Transport. Electrific.*, vol. 6, no. 3, pp. 935–947, Sep. 2020.

[9] G. Monti, F. Mastri, M. Mongiardo, L. Corchia, and L. Tarricone, "Load-independent operative regime for an inductive resonant WPT link in parallel configuration," *IEEE Trans. Microw. Theory Techn.*, vol. 68, no. 5, pp. 1809–1818, May 2020.

[10] L. He, J. Chen, B. Cheng, and H. Zhou, "Duty cycle loss compensation method based on magnetic flux cancelation in high-current high-frequency synchronous rectifier of LCLC converter," *IEEE Trans. Power Electron.*, vol. 36, no. 1, pp. 103–113, Jan. 2021.

[11] Z. Huang, S.-C. Wong, and C. K. Tse, "Control design for optimizing efficiency in inductive power transfer systems," *IEEE Trans. Power Electron.*, vol. 33, no. 5, pp. 4523–4534, May 2018.

[12] X. Qu, H. Chu, Z. Huang, S.-C. Wong, C. K. Tse, C. C. Mi, and X. Chen, "Wide design range of constant output current using double-sided LC compensation circuits for inductive-power-transfer applications," *IEEE Trans. Power Electron.*, vol. 34, no. 3, pp. 2364–2374, Mar. 2019.

[13] Y. H. Sohn, B. H. Choi, E. S. Lee, G. C. Lim, G. H. Cho, and C. T. Rim, "General unified analyses of two-capacitor inductive power transfer systems: Equivalence of current-source SS and SP compensations," *IEEE Trans. Power Electron.*, vol. 30, no. 11, pp. 6030–6045, Nov. 2015.

[14] Y. Li, J. Hu, M. Liu, Y. Chen, K. W. Chan, Z. He, and R. Mai, "Reconfigurable intermediate resonant circuit based WPT system with load-independent constant output current and voltage for charging battery," *IEEE Trans. Power Electron.*, vol. 34, no. 3, pp. 1988–1992, Mar. 2019.

[15] B. Cheng and L. He, "High-order network based general modeling method for improved transfer performance of the WPT system," *IEEE Trans. Power Electron.*, vol. 36, no. 11, pp. 12375–12388, Nov. 2021, doi: 10.1109/TPEL.2021.3076800.

[16] Z. Zhang, F. Zhu, D. Xu, P. T. Krein, and H. Ma, "An integrated inductive power transfer system design with a variable inductor for misalignment tolerance and battery charging applications," *IEEE Trans. Power Electron.*, vol. 35, no. 11, pp. 11544–11556, Nov. 2020.

[17] R. L. Steigerwald, "A comparison of half-bridge resonant converter topologies," *IEEE Trans. Power Electron.*, vol. 3, no. 2, pp. 174–182, Apr. 1988.

[18] H. Qiu, T. Sakurai, and M. Takamiya, "Digital transmitter coil for wireless power transfer robust against variation of distance and lateral misalignment," *IEEE Trans. Microw. Theory Techn.*, vol. 68, no. 9, pp. 4031–4039, Sep. 2020.

[19] R. Mai, Y. Chen, Y. Li, Y. Zhang, G. Cao, and Z. He, "Inductive power transfer for massive electric bicycles charging based on hybrid topology switching with a single inverter," *IEEE Trans. Power Electron.*, vol. 32, no. 8, pp. 5897–5906, Aug. 2017.

[20] Y. Li, Q. Xu, T. Lin, J. Hu, Z. He, and R. Mai, "Analysis and design of load-independent output current or output voltage of a three-coil wireless power transfer system," *IEEE Trans. Transport. Electrific.*, vol. 4, no. 2, pp. 364–375, Jun. 2018.

[21] J. Lu, G. Zhu, D. Lin, S.-C. Wong, and J. Jiang, "Load-independent voltage and current transfer characteristics of high-order resonant network in IPT system," *IEEE J. Emerg. Sel. Topics Power Electron.*, vol. 7, no. 1, pp. 422–436, Mar. 2019.

[22] L. Yang, X. Li, S. Liu, Z. Xu, C. Cai, and P. Guo, "Analysis and design of three-coil structure WPT system with constant output current and voltage for battery charging applications," *IEEE Access*, vol. 7, pp. 87334–87344, 2019.

[23] F. Liu, K. Chen, Z. Zhao, K. Li, and L. Yuan, "Transmitter-side control of both the CC and CV modes for the wireless EV charging system with the weak communication," *IEEE J. Emerg. Sel. Topics Power Electron.*, vol. 6, no. 2, pp. 955–965, Jun. 2018.

[24] Y.-G. Su, L. Chen, X.-Y. Wu, A. P. Hu, C.-S. Tang, and X. Dai, "Load and mutual inductance identification from the primary side of inductive power transfer system with parallel-tuned secondary power pickup," *IEEE Trans. Power Electron.*, vol. 33, no. 11, pp. 9952–9962, Nov. 2018.

[25] J. Yin, D. Lin, T. Parisini, and S. Y. R. Hui, "Front-end monitoring of the mutual inductance and load resistance in a series-series compensated wireless power transfer system," *IEEE Trans. Power Electron.*, vol. 31, no. 10, pp. 7339–7352, Oct. 2016.

[26] K. Song, Z. Li, J. Jiang, and C. Zhu, "Constant current/voltage charging operation for series-series and series-parallel compensated wireless power transfer systems employing primary-side controller," *IEEE Trans. Power Electron.*, vol. 33, no. 9, pp. 8065–8080, Sep. 2018.

[27] T. Nagashima, X. Wei, E. Bou, E. Alarcón, M. K. Kazimierczuk, and H. Sekiya, "Analysis and design of loosely inductive coupled wireless power transfer system based on class-E^2 DC-DC converter for efficiency enhancement," *IEEE Trans. Circuits Syst. I, Reg Papers*, vol. 62, no. 11, pp. 2781–2791, Nov. 2015.

[28] T. Nagashima, X. Wei, E. Bou, E. Alarcón, M. K. Kazimierczuk, and H. Sekiya, "Steady-state analysis of isolated class-E^2 converter outside nominal operation," *IEEE Trans. Ind. Electron.*, vol. 64, no. 4, pp. 3227–3238, Apr. 2017.

[29] J. Choi, D. Tsukiyama, Y. Tsuruda, and J. M. R. Davila, "High-frequency, high-power resonant inverter with eGaN FET for wireless power transfer," *IEEE Trans. Power Electron.*, vol. 33, no. 3, pp. 1890–1896, Mar. 2018.

[30] W.-X. Chen and Q.-H. Chen, "Application of class-E converter in magnetic resonant WPT system," in *Proc. IEEE Int. Conf. Aircr. Utility Syst. (AUS)*, Beijing, China, Oct. 2016, pp. 320–324.

[31] Z. Zhang, X. Zou, Z. Dong, Y. Zhou, and X. Ren, "A 10-MHz eGaN isolated class-Φ_2 DCX," *IEEE Trans. Power Electron.*, vol. 32, no. 3, pp. 2029–2040, Mar. 2017.

[32] Y. Wang, L. Dong, X. Liao, X. Ju, S. W. Su, and H. Ma, "A pulse energy injection inverter for the switch-mode inductive power transfer system," *IEEE Trans. Circuits Syst. I, Reg. Papers*, vol. 65, no. 7, pp. 2330–2340, Jul. 2018.

[33] S. Liu, M. Liu, S. Yang, C. Ma, and X. Zhu, "A novel design methodology for high-efficiency current-mode and voltage-mode class-E power amplifiers in wireless power transfer systems," *IEEE Trans. Power Electron.*, vol. 32, no. 6, pp. 4514–4523, Jun. 2017.

[34] S. Aldhaher, P.-K. Luk, A. Bati, and J. Whidborne, "Wireless power transfer using class E inverter with saturable DC-feed inductor," *IEEE Trans. Ind. Appl.*, vol. 50, no. 4, pp. 2710–2718, Jul./Aug. 2014.

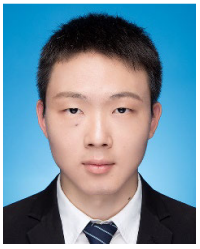

BING CHENG was born in Henan, China, in 1996. He received the B.E. degree from Xiamen University, Xiamen, China, in 2018, where he is currently pursuing the Ph.D. degree with the Department of Instrumental and Electrical Engineering. His research interests include wireless power transfer systems, DC/DC conversion topology, and switched controlled capacitor converters.

LIANGZONG HE was born in Hunan, China, in 1984. He received the B.Sc. degree from Jilin University, Changchun, China, in 2006, and the Ph.D. degree from the Huazhong University of Science and Technology, Wuhan, China, in 2012. From November 2009 to August 2011, he was a Joint Ph.D. Education Student with Michigan State University, East Lansing, MI, USA. In September 2012, he joined Xiamen University, Xiamen, China, as an Assistant Professor, where he has been a Professor, since August 2019. His research interests include high-efficient power conversion, DC-DC converters, switched-capacitor converters, Z-source converters, wireless power transmission, and battery management systems.